Relation between subcritical crack growth behavior and crack paths in granite

Y. NARA [a*], K. KOIKE [b], T. YONEDA [c] and K. KANEKO [d]

a. Dr. Eng., Division of Field Engineering for Environment, Graduate School of Engineering, Hokkaido University, Sapporo, JAPAN

(*Corresponding author, E-mail: nara@eng.hokudai.ac.jp, FAX: +81-11-706-6325)

b. Professor, Department of Civil and Environmental Engineering, Kumamoto University, Kumamoto, JAPAN

c. Professor, Division of Solid Waste, Resources and Geoenvironmental Engineering, Graduate School of Engineering, Hokkaido University, Sapporo, JAPAN

d. Professor, Division of Field Engineering for Environment, Graduate School of Engineering, Hokkaido University, Sapporo, JAPAN

1. Introduction

In fracture mechanics, crack growth occurs when the stress intensity factor at the crack tip reaches the fracture toughness [1, 2]. However, a crack can propagate even when the stress intensity factor is less than the fracture toughness. This phenomenon is called subcritical crack growth, and the main mechanism is stress corrosion [3, 4]. To ensure the long-term stability of structures in a rock mass, such as an underground power plant, a cavern for storing liquefied petroleum or natural gas (LPG or LNG), or a repository for radioactive wastes in underground, it is necessary to know the time-dependent behavior of the rock. Therefore, it is very important to study the problems of time-dependent rock deformation and fracturing.

We previously investigated subcritical crack growth in rock [5-8]. First, we showed how to estimate the activation energy for subcritical

crack growth in isotropic rock [7] using Double Torsion (DT) test [9]. Then, to extend this technique to anisotropic rock, especially granite, we presented a quantitative method for estimating the orthorhombic elastic constants and density of pre-existing microcracks [8, 10]. The elastic constants and crack density were used to analyze the subcritical crack growth behavior in granite. The activation energy for subcritical crack growth was estimated by considering the effect of pre-existing microcracks. Subcritical crack growth in granite was found to be dependent on the density of pre-existing microcracks, and cracks propagated by connecting with pre-existing microcracks ahead of the crack front. Since the density of microcracks ahead of the crack front was dependent on the crack propagation direction, the crack growth behavior could affect the geometry of the crack path.

It is necessary to verify the above analysis. Observations of the

crack path, which have been reported by several researchers, can be useful for investigating the effect of rock fabrics on crack growth behavior. For example, Swanson [11] observed crack paths for subcritical crack growth in Westerly granite and showed that the percentage of transgranular cracks tended to be higher in quartz, plagioclase, and biotite when the crack growth rate was higher. Kudo *et al*. [12] observed crack paths in Aji granite and investigated the interaction between the crack paths and mineral grains. The quartz grain played an important role as an obstacle; feldspar grain could change the direction of the crack paths because of its cleavage plane; and biotite grain had a significant effect on the crack paths even when its constitutive ratio was very small. However, the relation between the crack growth behavior and the geometry of the crack path is not clear from these studies.

This study aims at observing the crack paths obtained from DT tests

and investigating the relationship between the crack growth behavior and the geometry of the crack path. To estimate the geometry of the crack path, fractal analysis was performed and the crack lengths were measured.

2. Subcritical crack growth in granite

2.1 Mechanism of subcritical crack growth

Subcritical crack growth involves several competing mechanisms, such as stress corrosion, diffusion, ion exchange, and microplasticity. Under low homologous temperatures and atmospheric pressure, stress corrosion is the dominant mechanism [13]. For silicate materials, stress corrosion is expressed as [13, 14]

$$\equiv \mathrm{Si} - \mathrm{O} - \mathrm{Si} \equiv + \mathrm{H_2O} \rightarrow \equiv \mathrm{Si} - \mathrm{OH} + \mathrm{HO} - \mathrm{Si} \equiv . \qquad (1)$$

When stress corrosion controls the crack growth, the relation between the crack velocity, $\mathrm{d}a/\mathrm{d}t$, and the stress intensity factor, K_{I}, is

$$\frac{da}{dt} = v_0 P(H_2O) \exp\left(\frac{-E^{\ddagger} + \beta K_I}{RT}\right) \qquad (2)$$

where $P(H_2O)$ is the water vapor pressure, $E^{\ddagger}$ is the stress free activation energy, R is the gas constant, T is the absolute temperature, and v_0 and β are material constants [15-17]. Nara and Kaneko [8] considered the effect of pre-existing microcracks on the activation energy for granite using the equation

$$E^{\ddagger} = E_0^{\ddagger}(1 - \gamma \Phi_i) \qquad (3)$$

where $E_0^{\ddagger}$ is the activation energy of the granite matrix material, Φ_i is the crack density of microcracks parallel to the crack propagation direction, and γ is a constant [8].

2.2 Rock studied and Double Torsion specimens

The rock used for the DT tests and crack observations was Oshima granite from a quarry in Oshima, Ehime prefecture, in southwest Japan

[18]. This granite consists of quartz (36.4%), plagioclase (37.1%), potash-feldspar (22.2%), biotite (4.0%) and hornblende (0.3%), and the grain size is about 1 mm [19].

Oshima granite possesses orthorhombic elastic properties that are caused by the preferred orientation of pre-existing microcracks [20-22]. The P-wave velocities in the three orthogonal directions are listed in Table 1. The anisotropy of the P-wave velocity in Oshima granite is evident from this table. In this study, the orthogonal directions were called axis-1, -2, and -3 in the order of the measured P-wave velocities. The planes normal to axis-1, -2, and -3 were identified as plane-1, -2, and -3, respectively. These planes are consistent with the three splitting planes observed in the quarry; that is, plane-1, -2 and -3 are consistent with *Shiwa* (the hardway plane), *Niban* (the grain plane), and *Me* (the rift plane), respectively [23].

DT specimens were prepared, considering the crack propagation and opening directions, as shown in Fig. 1. In the 1•2-specimen, for example, the crack propagated in the direction parallel to axis-1 and opened parallel to axis-2.

A schematic illustration of a DT specimen and the loading configuration are shown in Fig. 2. In this study, $W = 45$ [mm], $L = 140 \sim 170$ [mm], $d = 3$ [mm], $d_n = 2$ [mm], $w_m = 18$ [mm], and the width of the guide groove was 1 mm. The size of the DT specimen satisfied the condition suggested by Pletka *et al*. [24], Evans *et al*. [25], and Atkinson [26] ($12d \le W \le L/2$).

Nara and Kaneko [8] have reported experimental results of DT tests for Oshima granite. They qualitatively showed the anisotropy of subcritical crack growth in granite due to the preferred orientation of pre-existing microcracks and the effects of temperature and water vapor

pressure. In addition, they found that the activation energy for granite was greater than that for glass. Nara and Kaneko suggested that this was due to the straight crack paths found in glass compared to the zigzag crack paths found in granite and was caused by the heterogeneity.

We correct here an error in Nara and Kaneko [8], where Appendix 2 was entitled “Calculation of the anisotropic elastic constants”. The title should be “Data about subcritical crack growth index”, which is suitable for the content of Appendix 2 in Nara and Kaneko [8].

3. Crack path observation

3.1 Observation method and procedure

After the DT tests were performed, the crack paths were observed by preparing polished thin sections. To obtain clear crack path images, backscattered-electron (BSE) composition images were used; these can be

obtained using a scanning electron microscope (SEM) or an electron probe microanalyzer (EPMA) [27-30]. However, it was probable that new cracks were created during the preparation of the thin sections. To avoid the effects of such cracks, fluorescent method [31-33] was also used in the analysis. Since a conductive coating is required to observe a specimen using SEM or EPMA, the fluorescent observations were made before obtaining the BSE images.

First, an epoxy resin with fluorescent paint was permeated into the cracks of the DT specimens. Then, polished thin sections were prepared to observe the tension plane (the lower plane in Fig. 2). The thickness of the thin section was 30 μm. The cracks were initially observed using an optical microscope with ultraviolet rays. An image obtained with the fluorescent method is shown in Fig. 3. In this figure, the length per pixel was 1.1 μm, while the length and height of the image were 1.5 and 0.9 mm,

respectively. The cracks induced while preparing the thin section do not appear in this image because the resin with fluorescent paint was allowed to penetrate the cracks before the preparation process.

After the cracks were observed using the fluorescent method, the surface of the polished thin section was coated with gold so that BSE images could be obtained with the EPMA. A BSE composition image obtained from the EPMA is shown in Fig. 4. In this image, the length per pixel was 0.6 μm, while the length and height of the image were 1.5 and 0.9 mm, respectively. The symbols Q, Pl, K, and Bt indicate quartz, plagioclase, potash-feldspar, and biotite, respectively.

In this study, the BSE images were used to extract the crack paths of subcritical crack growth because the cracks in these images were clearer. The fluorescent images were used to identify defects in the specimens that were introduced by means other than subcritical crack growth.

3.2 Analytical procedure

To estimate the geometry of the crack paths, they were transformed into digitized values. First, approximately 50 BSE images obtained from a single DT specimen were connected to cover the entire crack path. Only the crack path was extracted by the binary conversion process [34]. After thinning the binary images, the crack path was digitized. Spline interpolation was used to connect the interrupted parts of the crack path. Finally, a principal component analysis was used on the interpolated data.

Crack branching was often found, as shown in Figs. 3 and 4. In this study, only the main crack path, *i.e.*, the thicker and longer crack path, was analyzed. Isolated cracks were not analyzed.

The trace length of a typical crack path analyzed in this study was about 40 mm. The resolution of the digitized data of the crack path was

0.6 μm.

We describe the geometry of the crack path in two ways. The first description is in terms of the fractal dimension, which provided a scaling of the crack path roughness. The fractal dimensions were estimated using power spectrum-spatial frequency diagrams. The power spectrum of the crack path was calculated from Fast Fourier Transform (FFT) after applying Hanning's window. The relation between the power spectrum, $S(f)$, and the spatial frequency, f, for a fractal geometry can be expressed as [35]

$$S(f) \propto f^{-(5-2D)} \qquad (4)$$

where D is the fractal dimension, which can be calculated from the linear part of the power spectrum-frequency plot in log-log space.

The fractal analysis cannot be used to define the length of a crack. Therefore, the cracks were also described in terms of the trace length of

their paths, which was normalized by the distance between the start and end points of the digitized crack path. This was defined as the "normalized crack path length (NCL)", and indicates the roughness of the crack path.

The crack path analysis was conducted on two specimens for each opening plane. Hence, six specimens were used for the crack path analysis.

3.3 Results of the crack path observation

The digitized crack paths obtained using the procedure described in Section 3.2 are shown in Fig. 5. Figs. 5(a)-(c) indicate the path of a crack propagating parallel to plane-1, -2, and -3, respectively. The values of the fractal dimension and NCL were determined using these crack paths. One example of a power spectrum-spatial frequency diagram is shown in Fig.

6. The value of the fractal dimension was determined using Eq. (4) in the spatial frequency range from 10^1 to 10^3 m^{-1}, which corresponds to the grain size of Oshima granite.

The values of the fractal dimension *D* and NCL are summarized in Table 2, along with the results of the DT tests. In the table, $K_I(10^{-5})$ is the stress intensity factor at $da/dt = 10^{-5}$ [m/s] and d*a* / d*t* (1.8) is the crack velocity at $K_I = 1.8$ [$MN/m^{3/2}$]. The results showed that *D* and NCL tended to be smaller when the crack propagated parallel to plane-3, which had the highest density of pre-existing microcracks and the lowest activation energy. Therefore, the anisotropic properties and activation energy of subcritical crack growth in granite were related to the roughness of the crack path.

4. Discussion

The values of the fractal dimension and NCL were smallest when the crack grew parallel to plane-3. This was caused by the fact that the crack propagated via connecting microcracks in the granite. If the crack propagated parallel to plane-3, there were many microcracks parallel to the crack propagation direction. Then, the distance from the crack tip to the nearest microcrack parallel to the crack propagation direction tended to be small because of the high density of pre-existing microcracks. As a result, the crack connected easily with the microcracks and the crack path became smooth, resulting in lower fractal dimension and NCL values.

Conversely, if there were few microcracks parallel to the crack propagation direction, the distance from the crack front to the nearest microcrack tended to be longer. Therefore, the crack propagated along a curving path, creating a complicated geometry. Consequently, the density

of pre-existing microcracks affected the roughness of the crack path.

The difference in crack path roughness discussed above is in harmony with the activation energy of subcritical crack growth in granite. From Table 2, as the crack path became smoother, the activation energy decreased. This result is consistent with the findings of Nara and Kaneko [8] regarding the difference between the activation energies of glass and rocks. The same was true for different crack propagation directions in the same material: the roughness, or the surface area of the crack path, affected the activation energy. In granite, the preferred orientation of the pre-existing microcracks created different surface energies for the crack paths. Therefore, the preferred orientation of the microcracks caused the differences between the activation energies of subcritical crack growth in granite.

Branching cracks can cause differences in the surface area of the

crack paths created during subcritical crack growth. This effect must also be considered. The number of branching cracks from the main crack path is listed in Table 3. The number of branching cracks was the smallest when the crack propagated parallel to plane-3, while the number of branching cracks was the largest when the crack propagated parallel to plane-1. Therefore, crack branching did not cause the differences in the surface energy of the crack paths in different crack propagation directions, and it is appropriate to discuss differences in the geometry of the main crack path.

5. Conclusions

In this study, stress-induced crack paths were observed after DT tests were performed to investigate the relationship between crack paths and crack growth behavior. Crack paths were observed using an EPMA,

and the geometry of the crack paths was estimated quantitatively from a fractal analysis and crack length determination process.

The fractal dimension and normalized crack path length were the lowest for crack paths parallel to plane-3. This was because the geometry of the crack path was smooth when the crack propagated parallel to the plane in which the density of microcracks was high. From the results of the DT tests and crack path analysis, it was shown that the crack density and preferred orientation of the pre-existing microcracks affected the crack growth behavior. The differences between the activation energies of subcritical crack growth in granite were caused by the preferred orientation of the pre-existing microcracks.

References

[1] Griffith, AA. The phenomena of rupture and flow in solids. Phil. Trans. Roy. Soc. 1920; 221: 163-198.

[2] Irwin, GR. Analysis of stresses and strains near the end of a crack transversing a plate. J. Appl. Mech. 1957; 24: 361-64.

[3] Anderson, OL and Grew, PC. Stress corrosion theory of crack propagation with applications to geophysics. Rev. Geophys. Space Phys. 1977; 15: 77-104.

[4] Atkinson, BK. Subcritical crack propagation in rocks: theory, experimental results and applications. J. Struct. Geol. 1982; 4: 41-56.

[5] Nara, Y, Ohno, Y, Imai, Y, and Kaneko, K. Anisotropy and grain-size dependency of crack growth due to stress corrosion in granite. Shigen-to-Sozai 2004; 120: 25-31 [in Japanese with English

abstract].

[6] Nara, Y, Imai, Y, and Kaneko, K. Dependence of subcritical crack growth on rock fabric and environment. Shigen-to-Sozai 2004; 120: 431-39 [in Japanese with English abstract].

[7] Nara, Y and Kaneko, K. Study of subcritical crack growth in andesite using the Double Torsion test. Int. J. Rock Mech. Min. Sci. 2005; 42: 521-30.

[8] Nara, Y and Kaneko, K. Subcritical crack growth in anisotropic rock. Int. J. Rock Mech. Min. Sci. 2005; 43: 437-453.

[9] Evans, AG. A method for evaluating the time-dependent failure characteristics of brittle materials and its applications to polycrystalline alumina. J. Mater. Sci. 1972; 7: 1137-46.

[10] Nara, Y and Kaneko, K. Evaluation of the elastic constants of granite. Shigen-to-Sozai 2003; 119: 396-402 [in Japanese with

English abstract].

[11] Swanson, PL. Subcritical crack fracture propagation in rocks: an examination using the methods of fracture mechanics and nondestructive testing. PhD. Thesis, University of Colorado, 1985.

[12] Kudo, Y, Sano, O, Murashige, N, and Mizuta, Y. Stress-induced crack path in Aji granite under tensile stress. PAGEOPH 1992; 138: 641-56.

[13] Atkinson, BK and Meredith, PG. The theory of subcritical crack growth with applications to minerals and rocks, in *Fracture mechanics of rock*. London: Academic Press; 1987. p. 111-166.

[14] Michalske, TA and Freiman, SW. A molecular interpretation of stress corrosion in silica. Nature 1982; 295: 511-2.

[15] Wiederhorn, SM. Influence of water vapor on crack propagation in soda-lime glass. J. Am. Ceram. Soc. 1967; 50: 407-14.

[16] Soga, N, Okamoto, T, Hanada, T, and Kunugi, M. Chemical reaction between water vapor and stressed glass. J. Am. Ceram. Soc. 1979; 62: 309-10.

[17] Wiederhorn, SM, Fuller, ER Jr, and Thomson, R. Micromechanisms of crack growth in ceramics and glasses in corrosive environments. Met. Sci. 1980; 14: 450-8.

[18] Hisanaga, K, Kudo, Y, Sano, O, and Nakagawa, K. Preferred orientation of granite joints in Oshima, Southwest Japan. Proceedings of the International Symposium on Assessment and Prevention of Failure Phenomena in Rock Engineering, Istanbul, Turkey, 1993. p. 543-547.

[19] Sano, O, Ito, I, and Terada, M. Influence of strain rate on dilatancy and strength of Oshima granite under uniaxial compression. J. Geophys. Res. 1981; 86: 9299-311.

[20] Sano, O, Kudo, Y, and Mizuta, Y. Experimental determination of elastic constants of Oshima granite, Barre granite and Chelmsford granite. J. Geophys. Res. 1992; 97: 3367-79.

[21] Peacock, S, McCann, C, Sothcott, J, and Astin, TR. Seismic velocities in fractured rocks: an experimental verification of Hudson's theory. Geophys. Prospecting 1994; 42: 27-80.

[22] Takemura, T, Golshani, A, Oda, M, and Suzuki, K. Preferred orientations of open microcracks in granite and their relation with anisotropic elasticity. Int. J. Rock Mech. Min. Sci. 2003; 40: 443-54.

[23] Kudo, Y, Hashimoto, K, Sano, O, and Nakagawa, K. Relation between physical anisotropy and microstructures of granitic rock in Japan. Proceedings of the 6th International Congress on Rock Mechanics, Montreal, Canada, 1987. p. 429-32.

[24] Pletka, BJ, Fuller, ER Jr, and Koepke, BG. An evaluation of

double-torsion testing – Experimental. ASTM STP, Vol. 678, 1979. p. 19-37.

[25] Evans, AG, Linzer, M, and Russell, LR. Acoustic emission and crack propagation in polycrystalline alumina. Mater. Sci. Eng. 1974; 15: 253-61.

[26] Atkinson, BK. Fracture toughness of Tennessee sandstone and Carrara marble using the double torsion testing method. Int. J. Rock. Mech. Min. Sci. Geomech. Abstr. 1979; 16: 46-53.

[27] Robinson, BW and Nickel, EH. A useful new technique for mineralogy: the backscattered-electron/low vacuum mode of SEM operation. Am. Mineral 1979; 64: 1322-8.

[28] Hall, MG and Lloyd, GE. The SEM examination of geological samples with a semiconductor back-scattered electron detector. Am. Mineral 1981; 66: 362-8.

[29] Kanaori, Y, Yairi, K, and Ishida, T. Grain boundary microcracking of granitic rocks from the northeastern region of the Atotsugawa fault, central Japan: SEM backscattered electron images. Eng. Geol. 1991; 30: 221-35.

[30] Krinsley, DH, Pye, K, Boggs, S Jr, and Tovey, NK. Backscattered scanning electron microscopy and image analysis of sediments and sedimentary rocks. New York: Cambridge University Press; 1998.

[31] Gardner, RD and Pincus, HJ. Fluorescent dye penetrants applied to rock fractures. Int. J. Rock Mech. Min. Sci. 1968; 5: 155-8.

[32] Ali, SA and Weiss, MP. Fluorescent dye penetrant technique for displaying obscure structures in limestone. J. Sediment Petrol 1968; 38: 681-2.

[33] Nishiyama, T and Kusuda, H. Identification of pore spaces and microcracks using fluorescent resins. Int. J. Rock Mech. Min. Sci.

Geomech. Abstr. 1994; 31: 369-75.

[34] Kitteler, J and Illingworth, J. Minimum Error Thresholding. Pattern Recognit. 1986; 19: 41-7.

[35] Mandelbrot, BB. The fractal geometry of nature. New York: W. H. Freeman and Company; 1983.

Table 1　The P-wave velocities for Oshima granite.

Direction	axis-1	axis-2	axis-3
P-wave velocity [km/s]	4.91	4.61	4.51

Table 2　Summary of the results of the crack path analysis and DT test. NCL, D, and $E^{\ddagger}$ mean normalized crack path length, fractal dimension, and activation energy, respectively.

opening plane	specimen	NCL	average of NCL	D	average of D	$K_I(10^{-5})$ [$MN/m^{3/2}$]	da/dt(1.8) [m/s]	$E^{\ddagger}$ [kJ/mol]
plane−1	2・1	1.43	1.36	1.57	1.40	1.99	$1.01*10^{-8}$	173
	3・1	1.28		1.22				
plane−2	1・2	1.28	1.29	1.10	1.08	1.82	$5.01*10^{-6}$	159
	3・2	1.29		1.05				
plane−3	2・3	1.27	1.26	1.09	1.07	1.73	$2.55*10^{-4}$	154
	1・3	1.25		1.05				

Table 3　The number of branching cracks from the main crack path.

opening plane	specimen	The number of branching	average
plane−1	2・1	32	30
	3・1	28	
plane−2	1・2	28	26
	3・2	23	
plane−3	2・3	23	23
	1・3	22	

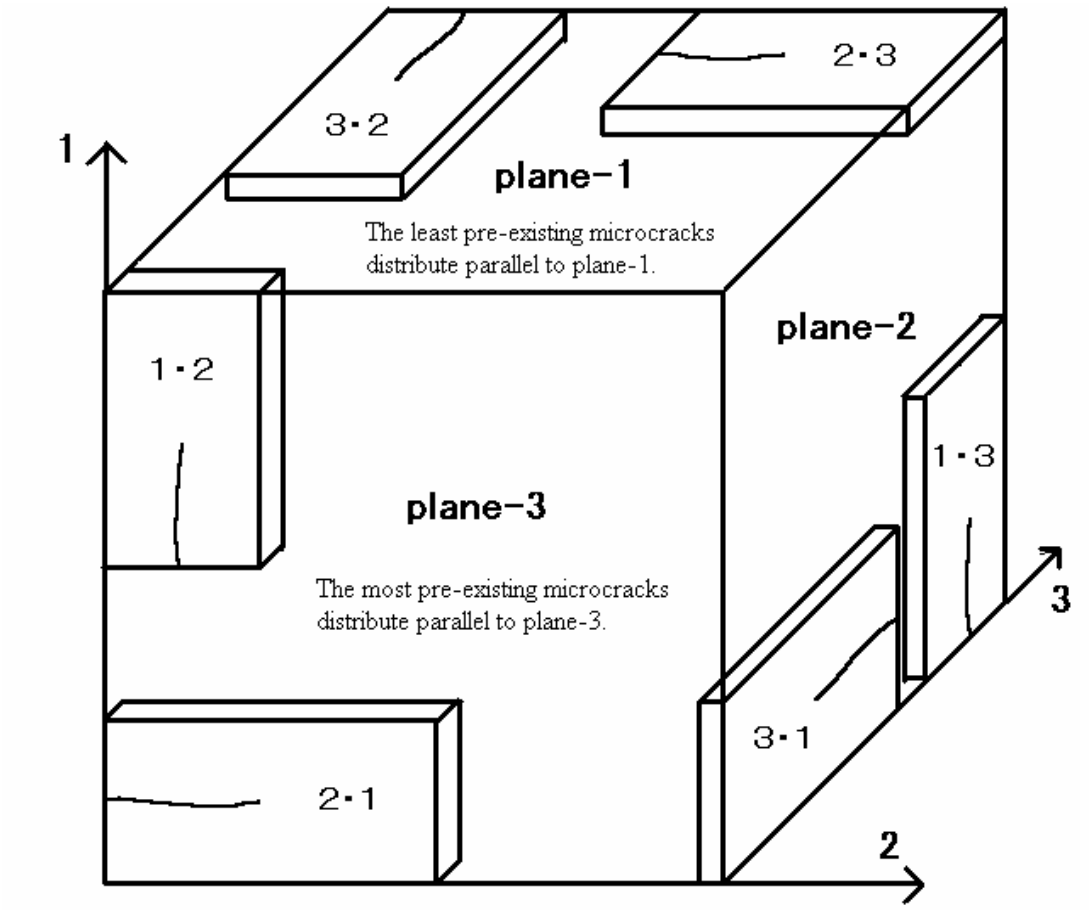

Fig.1　A schematic view of the specimen orientations. The least or most pre-existing microcracks distribute parallel to plane-1 or plane-3, respectively.

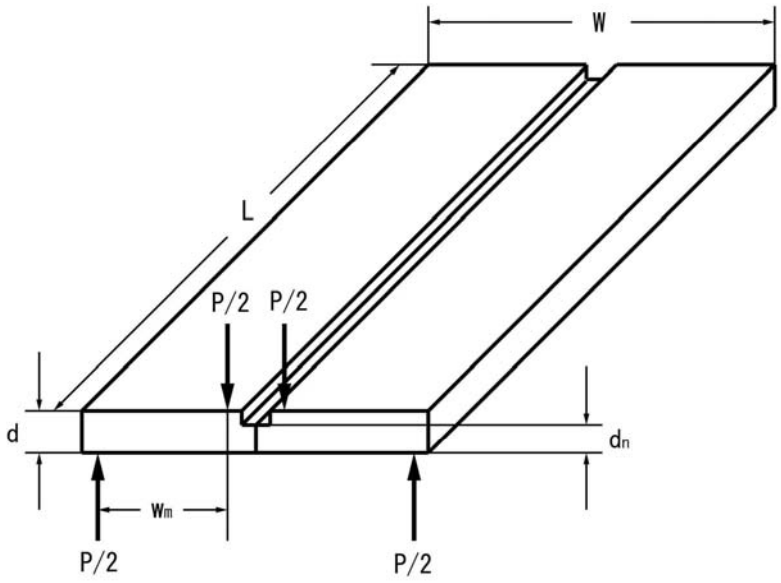

Fig. 2　Double Torsion specimen and the loading configuration.

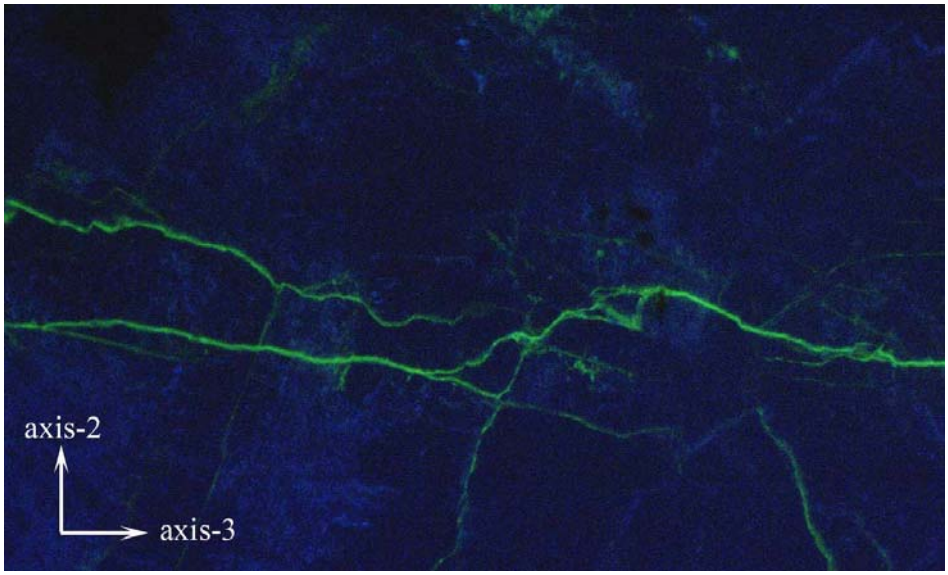

Fig. 3　A crack path image obtained using a fluorescent method.
In this specimen, the crack propagation direction is parallel to axis-3 and the opening direction is parallel to axis-2.
The length and height of the image are 1.5 mm and 0.9 mm.

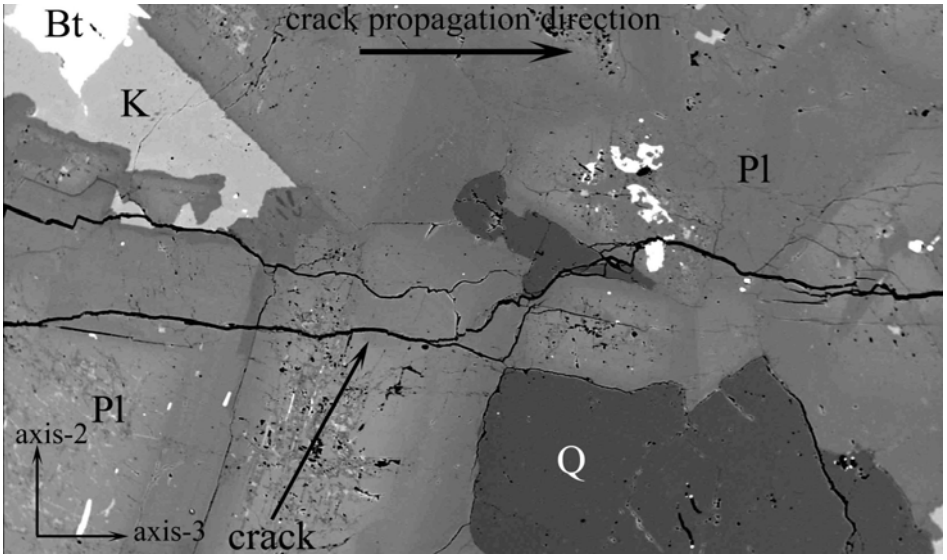

Fig. 4　A crack path in BSE image.　In this specimen, the crack propagation direction is parallel to axis-3 and the opening direction is parallel to axis-2.
The length and height of the image are 1.5 mm and 0.9 mm.
Q：quartz, Pl：plagioclase, K：potash feldspar, Bt：biotite.

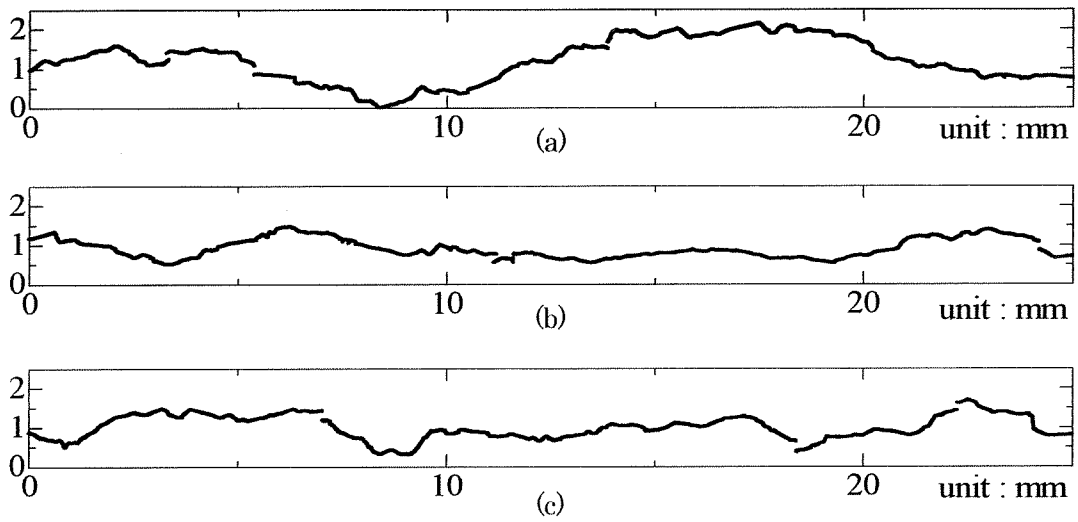

Fig. 5 The stress-induced crack paths for Oshima granite.
(a) : The crack propagated parallel to plane-1 (Specimen 3•1).
(b) : The crack propagated parallel to plane-2 (Specimen 1•2).
(c) : The crack propagated parallel to plane-3 (Specimen 1•3).

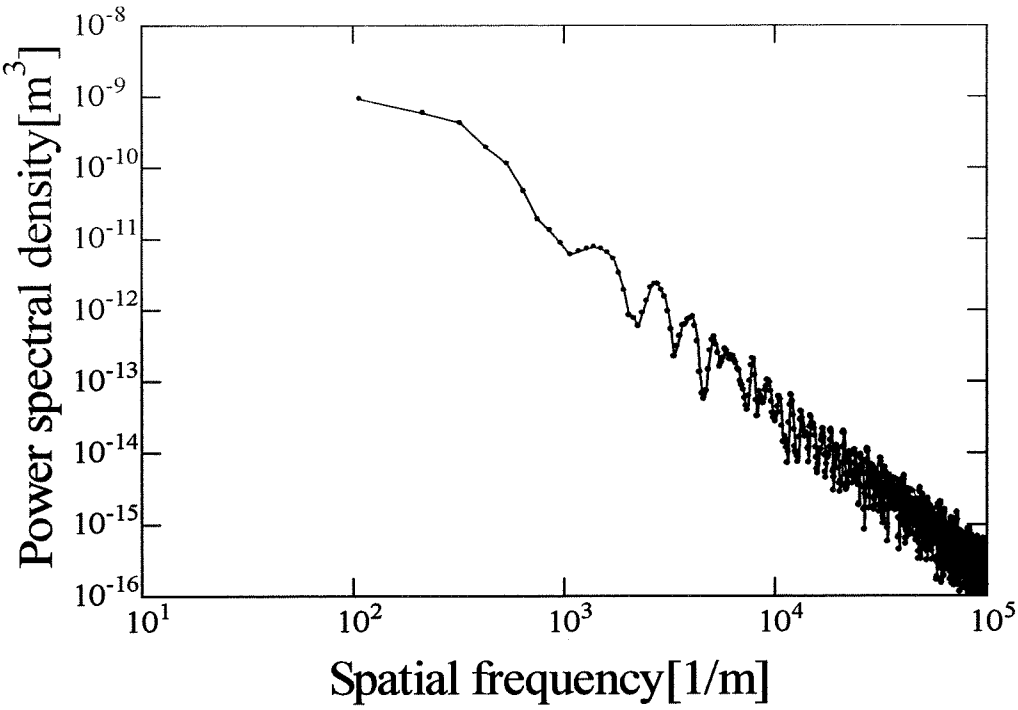

Fig. 6 The power spectrum of the crack path (Specimen 2•3).